



High variability of interaction energy between volcanic particles: implications for deposit stability

Alfonso Ontiveros-Ortega^{1,2} · Iban Plaza¹ · Julio Calero³ · Jose Alberto Moleon¹ · Jesús Miguel Ibañez^{2,4}

Received: 22 July 2022 / Accepted: 17 April 2023
© The Author(s) 2023

Abstract

Landslides on the flanks of stratovolcanoes can significantly modify the structure of the volcano. Macroscopic factors that determine the stability of volcanic deposits are well understood, but the microscopic interactions between particles and their impact on deposit cohesion remain poorly understood. Deposit cohesion is related to the energy of interaction between particles, and its calculation depends on the surficial properties of the eruptive materials. The purpose of this study was to perform a preliminary comparative analysis of the surficial properties of volcanic materials from various tectonic settings, including electrical (zeta potential) and thermodynamic (surface free energy) components and to calculate the total interaction energy between particles under different environmental conditions. We analyzed samples of eruptive materials obtained from volcanic flows characteristic of six active volcanoes (El Hierro, Pico Do Fogo, Vulcano, Stromboli, Mt. Etna, and Deception Island). The results show that deposit cohesion varies among volcanoes and changes drastically with the pH of the medium. Among the volcanic systems investigated, El Hierro (pH=3) has the most cohesive materials, while Mt. Etna (pH=8) has the least cohesive materials. Our results suggest that microscopic electrical and thermodynamic properties play a role in the stability of volcanic deposits, and confirm the need for a greater research focus in this area.

Keywords Zeta potential and surface free energy · Volcanic ashes · Interaction energy between colloidal particles

✉ Alfonso Ontiveros-Ortega
aontiver@ujaen.es

¹ Department of Physics, University of Jaén, Jaén, Spain

² Andalusian Institute of Geophysics, University of Granada, Granada, Spain

³ Department of Geology, University of Jaén, Jaén, Spain

⁴ Department of Theoretical Physics, University of Granada, Granada, Spain

1 Introduction

Volcanic structures are complex, and landslides formed of unconsolidated eruptive deposits constitute a significant natural hazard, particularly where heavy rainfall can produce soil sliding (Bommer et al. 2002). Mitigation of landslide hazards in such regions requires a thorough understanding of the behavior of volcanic soils under static and dynamic conditions. The cohesion and stability of volcanic deposits depend on the environmental conditions (e.g., rainfall, fumarolic activity, etc.) and on their chemistry [e.g., pH or concentration of salts; (Li et al. 1997; Voight and Elsworth 1997; Ontiveros-Ortega et al. 2016; Plaza et al. 2018)]. The microscopic structure of soil is determined by adhesion between different particles, chemical group absorption, coagulation between similar substances, and heterocoagulation between different substances (Ontiveros-Ortega et al. 2016, 2018; Plaza et al. 2018). That is, the cohesion and stability of a volcanic deposit at the macroscopic level depends directly on the microscopic surface properties of the eruptive materials from which it is formed.

The analysis of surface properties and the study of solid–liquid interfaces are important within a wide range of problems in applied colloidal science. Wettability, adsorption, adhesion, and cohesion all largely depend on the electrical properties and surface free energy of the material (Li et al. 1997; Ontiveros-Ortega et al. 2016; Plaza et al. 2018; Aizawa 2008; Aizawa et al. 2008; Gimmi and Kosakowski 2011; Baumgarten et al. 2013; Kadar et al. 2014). Charge generation along the particle–water interface, as well as thermodynamic surface properties, is related to chemical groups on particle surfaces. The generation of these groups depends on the chemical nature of the material, including the composition, mineralogy, and crystalline structure (Aizawa 2008) and the ash's history of interaction with gases or aerosols in the eruption plume (Maters et al. 2016).

Volcanic environments often experience significant rainfall, which results in the washing of deposits; at the same time, hydrothermal processes and gas emissions deposit large volumes of salts, heavy metals, and other substances. These processes affect the surface physical–chemical properties of the material and can facilitate the dissolution and leaching of volcanic glass (Dultz et al. 2016). Together, this results in modification of the ionic medium and the pH of the deposit, which will have an effect on the cohesion and degree of hydrophobicity or hydrophilicity of the deposits and will thus condition their capacity to retain water and the stability of the volcanic structure.

The objective of this work was to perform a preliminary comparative study of the surface properties of tephra. These properties are determined to interpret flocculation, adsorption, wetting phenomena, and rheological properties of suspended materials in water solution (Ontiveros-Ortega et al. 2016; Bailey et al. 2014; Plaza et al. 2015; Kelly et al. 2010). We analyzed the electrical and thermodynamic properties of tephra samples from six different active volcanoes with different chemical characteristics, and we estimate the cohesion of the deposits as a function of environmental conditions. We believe that this is the first study of its kind, and while the results are limited to a small sample set, they confirm the utility of the approach and reveal the potential for further research in this area.

2 Methods

2.1 Compositional and textural characterization

Whole rock sample compositions were analyzed by wavelength-dispersive X-ray fluorescence (XRF) using an S4 Pioneer Prior XRF (Bruker AXS Inc., Madison, Wisconsin, USA) (at the Jaén University). Prior to analysis, samples were washed in distilled water and left to dry at a temperature of 343°K over 48 h. Then, samples were crushed using an agate mortar to ensure a uniform texture and particle size distribution and then pressed into tablet form using a hydraulic press (model MIGNON SS, Nannetti, Faenza, Italy). Although crushing the samples alters the surface physicochemical properties of the volcanic materials, as present in the environment, this was required by the analysis techniques employed. All reagents and chemicals were of analytical grade (Merck KGaA and Sigma-Aldrich Co. LLC, Germany).

Scanning electron microscope (SEM) imagery was used to document sample textures, including the distribution of vesicles and presence of volcanic glass (Holtz et al. 1981). SEM images were collected using a Hitachi S-510 (Hitachi Ltd., Tokyo, Japan) with an acceleration voltage of 25 kV. Prior to analysis, samples were coated with colloidal silver and carbon deposited in two orientations (20° and 30°).

2.2 Zeta potential

The samples have been crushed and sieved, leaving us with a size of less than 1 mm. They have not been washed and have been conditioned with each electrolytic solution for 24 h. To study the electrical surface properties of the crushed volcanic material, we have used the zeta potential (ξ), parameter determined by the particles surface charge. To obtain zeta potential, dissolutions of electrolytes were prepared with an NaCl concentration of 1 mM and a small quantity of ground sample (0.05 g). This suspension (20 ml) was mechanically agitated, and the pH was adjusted between 3 and 9 using NaOH and HCl additions. Upon fitting with the pH measurements, we obtained ξ values of electrophoretic mobility at 20.0 °C \pm 0.5 °C in a Malvern Zetasizer 3000 HS; ξ was calculated based on the Smoluchowski approximation (Smoluchowski 1921).

2.3 Surface free energy determination

To determine surface free energy, we used the thick-layer wicking method. This is based on measurement of the time t that a liquid of viscosity η and surface tension γ^3 takes to penetrate a distance x through a thin, porous wall of a volcanic ash sample. The description of the process is given by a generalized form of Eq. 1 (Washburn 1921; Chibowski 1992; Chibowski and Holysz 1992; Duran et al. 1998; Ontiveros-Ortega et al. 2014):

$$x^2 = \frac{rt}{2\eta} \Delta G \quad (1)$$

where ΔG is the change in free energy associated with the replacement of a solid/air interface by a solid/liquid one in the wicking process, and r is the effective mean radius of the capillary network forming the thin layer of solid.

Spontaneous wicking occurs if $\Delta G > 0$. It has been shown that ΔG is related to the solid surface free energy components, dependent on experimental conditions considered in the wicking process. The experimental procedure was as follows. Capillaries of 1 mm in diameter were filled with the different ash samples and dried for 24 h at room temperature. Then, they were either oven-dried at 110 °C for 1 h and stored in a desiccator (“bare plates”) or put into contact with the vapor of the liquid used in the wicking experiments in a closed chamber for several hours (“precontacted plates”). Liquids used for the experiments were water, formamide, and *n*-decane. Surface tension and its components of the liquids were taken from the literature and are shown in Table 1. The time required for the liquids to permeate a given distance of both bare and precontacted plates was measured to obtain surface free energy components of the ash (Chibowski and Holysz 1992). The powdered ash was previously equilibrated over 24 h with electrolyte solutions at the desired concentration (1 mM) at natural pH. For brevity, we do not describe this in detail; the reader is instead directed to the literature associated with Washburn’s equation (e.g., Washburn 1921; Chibowski and Holysz 1992; Duran et al. 1998; Ontiveros-Ortega et al. 2014).

2.4 Calculation of interaction energy

The adhesion between solid particles of colloidal size dispersed in aqueous media is determined by the balance of forces between various phases coexistent in a system—namely, hydrodynamic, diffusive type, and interfacial. The first two are used for the approximation of particles and short distances (up to 100 nm), while interfacial forces act at distances more than 100 nm. These are electrical interactions between two layers, as well Lifshitz-van der Waals (LW) and acid–base (AB) interactions between condensed phases.

According to the so-called extended Derjaguin–Landau–Verwey–Overbeek (or DLVO) theory (Oss et al. 1988, 1989; Oss 1994), three types of interfacial interactions should be considered: LW, electrostatic (EL), and AB. For particles (phase 1) of the same material dispersed in water (phase 3), the total interaction energy between particles is given by:

$$\Delta G_{131}^{\text{TOT}} = \Delta G_{131}^{\text{EL}} + \Delta G_{131}^{\text{LW}} + \Delta G_{131}^{\text{AB}}, \quad (2)$$

where subscript 131 refers to the phases involved. In our case, 131 in ΔG_{131} refers to the particle–liquid medium–particle in the aggregation process:

$$\Delta G_{131}^{\text{EL}} = 2\pi\epsilon a\zeta^2 \ln(1 + e^{-\kappa H}) \quad (3)$$

Table 1 Surface tension and its components (mJ/m²) of liquids used in contact angle and thin-layer wicking measurements [taken from van Oss (1994)]

Liquid	γ	γ^{LW}	γ^+	γ^-
<i>n</i> -Decane	23.8	23.8	0	0
Formamide	58.0	39.0	2.28	39.6
Water	72.8	21.8	25.5	25.5

$$\Delta G_{131}^{\text{LW}} = -\frac{A_{131}}{6} \left(\frac{2a^2}{H(4a+H)} + \frac{2a^2}{(2a+H)^2} + \ln \frac{H(4a+H)}{(2a+H)^2} \right) \quad (4)$$

where a is the particle radius, H is distance between particles, ϵ is the dielectric constant of the liquid, κ is the Debye screening length (double-layer thickness), and A_{131} is the Hamaker constant for each system, which can be estimated by surface tension determination for the materials involved. Using the approximations proposed by van Oss (1994), the surface free energy (or surface tension) γ_i of a condensed phase consists of two additive contributions, dispersive LW and polar AB, which in turn depend on two parameters accounting for the electron-donor (γ^-) and electron-acceptor (γ^+) characteristics of the material ($\gamma_i = 2(\gamma_i^+ \gamma_i^-)^{1/2}$). If γ_i^{LW} is known for all of the phases involved, the Hamaker constant can be obtained as:

$$A_{131} = 12\pi H_0^2 \Delta G_{131,H_0}^{\text{LW}} \quad (5)$$

$$\Delta G_{131,H_0}^{\text{LW}} = -2 \left(\sqrt{\gamma_1^{\text{LW}}} - \sqrt{\gamma_3^{\text{LW}}} \right)^2 \quad (6)$$

where H_0 is estimated at $1.58 \pm 0.08 \text{ \AA}$ (van Oss et al. 1988).

Similarly, calculation of the H dependence of $\Delta G_{131}^{\text{AB}}$ requires knowledge of γ^+ and γ^- for the two phases and is given as:

$$\Delta G_{131}^{\text{AB}} = 2\pi a \lambda \Delta G_{131,H_0}^{\text{AB}} e^{\left(\frac{H_0-H}{\lambda} \right)} \quad (7)$$

where λ is the correlation length of water molecules (approximately, $\lambda = 1 \text{ nm}$ for hydrophilic surfaces), and ΔG_{131} depends on the AB parameters of the free energy of phases 1 (particle) and 3 (see Table 1 for water (Ontiveros-Ortega et al. 2016; Oss 1994)). According to van Oss, the quantity $\Delta G_{131}^{\text{AB}}, H_0$ is given as:

$$\Delta G_{131,H_0}^{\text{AB}} = -4 \left(\sqrt{\gamma_1^+ \gamma_1^-} + \sqrt{\gamma_3^+ \gamma_3^-} - \sqrt{\gamma_1^+ \gamma_3^-} - \sqrt{\gamma_3^+ \gamma_1^-} \right) \quad (8)$$

3 Materials

We analyzed ashes samples data from six volcanoes situated within two broad geotectonic environments: back-arc subduction/rifting related (Vulcano, Stromboli and Mt. Etna, Italy, Deception Island, in Antarctica) and intra-plate (Pico Do Fogo in Cape Verde, and El Hierro in the Canary Islands of Spain). Table 2 provides details of the volcanoes investigated in this study; Table 3 provides compositional information based on XRF whole rock analysis. A map of volcano locations is provided in Fig. 1; Fig. 2 shows the classification of samples based on total alkali ($\text{NaO} + \text{K}_2\text{O}$) versus silica compositions (i.e., a TAS diagram); SEM images of typical sample textures are shown in Fig. 3.

Table 2 Basic data of the samples: GPS location, altitude, regional tectonics, VEI (Volcanic Explosivity Index) and type of eruption

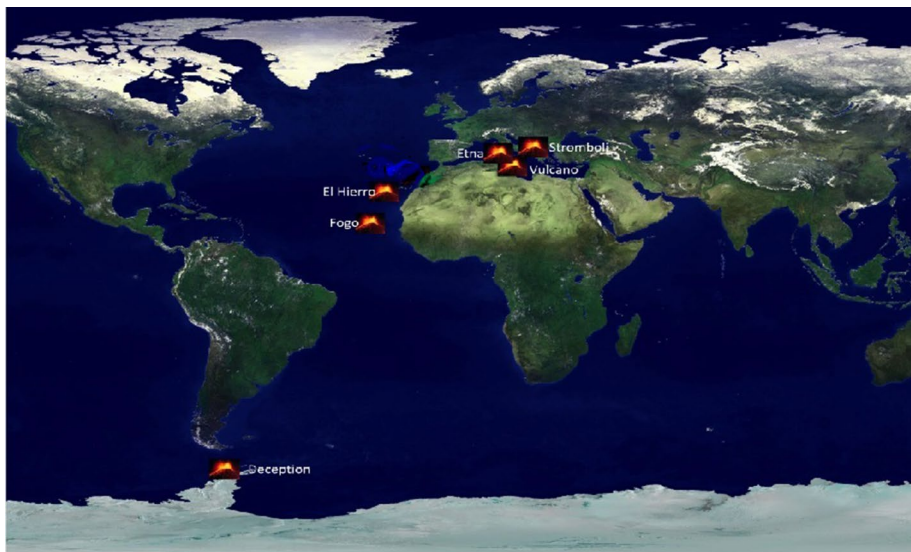
Volcanoes	Coordinates (UTM)		Altitude (m)	Tectonics	VEI	Eruptions date	Eruption type
El Hierro	27° 43' 22.42" N	18° 3' 45.58" O	1046	Interplate-Oceanic C. < 15 km	1/2	–	Hawaiian/Strombolian
Fogo	14° 56' 55.36" N	24° 20' 29.32" O	2731	Interplate-middle C. 15–25 km	1	1995	Hawaiian
Vulcano	38° 24' 15.76" N	14° 58' 0.670" E	321	Subduction Convection > 25 km	3	1890	Vulcanian
Stromboli	38° 47' 45.10" N	15° 13' 22.17" E	538	Subduction Convection > 25 km	2	–	Strombolian
Etna	37° 42' 21.94" N	15° 00' 15.83" E	2053	Subduction Convection > 25 km	2	1699	Strombolian
Deception	62° 58' 4.37" S	60° 33' 35.02" O	225	Divergent Limit—Continental Crust > 25 km	3	1969	Phreatomagmatic

From: the Smithsonian Institution's Global Volcanism Program (GVP) is housed in the Department of Mineral Sciences, National Museum of Natural History, in Washington D.C. <http://volcano.si.edu>

Table 3 X-ray fluorescence (XRF) analysis for different studied volcanic deposits (% oxide)

Oxides	Vulcano	Deception	Stromboli	Etna	El Hierro	Fogo
SiO ₂	58.50	54.20	51.70	47.90	43.30	42.80
Al ₂ O ₃	15.60	15.00	13.90	14.10	14.10	14.60
LOI*	1.46	6.70	0.17	0.19	0.59	0.18
Na ₂ O	3.38	4.08	1.40	1.93	2.72	2.88
K ₂ O	4.87	0.69	2.00	1.44	1.58	2.16
Fe ₂ O ₃	5.81	9.49	9.56	11.17	12.94	11.49
CaO	4.93	7.05	11.60	12.50	11.00	11.40
MgO	2.86	3.39	8.85	8.58	5.55	6.97
TiO ₂	0.41	1.71	0.83	1.48	4.45	3.09
Cl	0.09	–		–	–	–
SO ₃	0.22	–		0.04	0.10	0.10
MnO	0.09	0.15	0.16	0.15	0.16	0.15
P ₂ O ₅	0.35	0.30	0.52	0.39	1.00	0.88
ZrO ₂	–	0.04	0.02	0.02	0.05	0.00
SrO	0.01	0.03	0.063	0.09	0.11	0.02
Total	98.59	102.82	100.78	99.98	97.64	96.72

*Loss on ignition

**Fig. 1** Map showing the locations of the volcanoes studied

3.1 El Hierro, Spain

El Hierro is located within the Canary Islands, where four islands and seven islets are linked to a hotspot beneath a transitional area between oceanic crust and the African continent (Guillou et al. 1996). The geologic history of the island has been described by

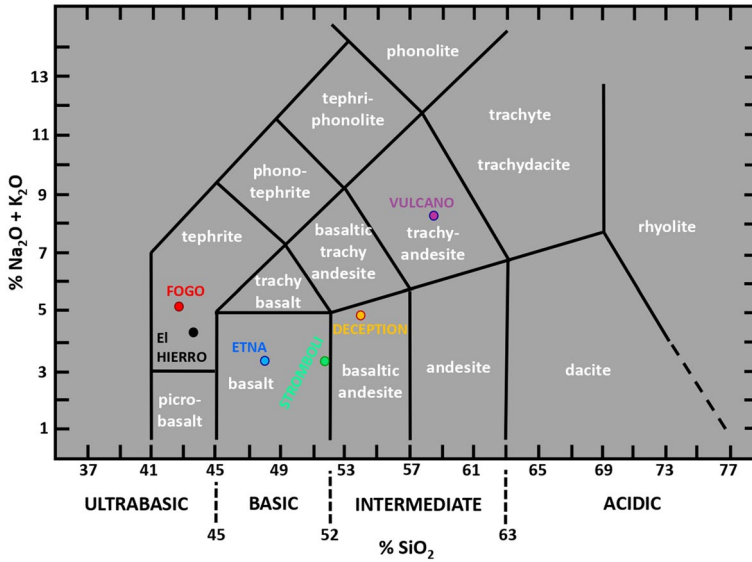


Fig. 2 Classification of studied of volcanic samples according to the total alkali versus silica (TAS) diagram

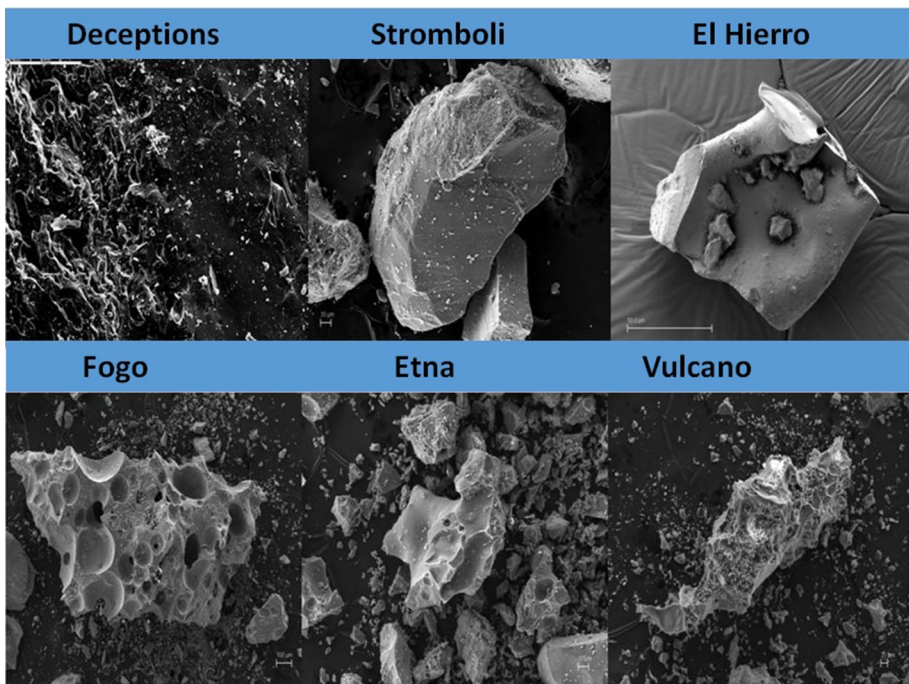


Fig. 3 Scanning electron microscope (SEM) images of the volcanic ash studied

different authors (e.g., Ancochea et al. 1990). The island is experiencing the on-going collapse of its principal structure (Carracedo et al. 2002); landslides are frequent and have large dimensions (Siebert et al. 2010).

The sample was taken from a cineritic level of black color, fresh appearance, and very little consolidation. Balcells and Gomez (1997b) associated the presence of this very fine-grained level with pulses or phreatomagmatic phases linked to purely magmatic monogenic eruptions around the northwest ridge summits of the island. Based on the TAS classification diagram, the samples can be classified as tephrite. SEM images show that the samples are vesicle-poor, indicative of a gentle eruption style.

3.2 Pico Do Fogo, Cape Verde

The Cape Verde islands are situated within the same broad tectonic context as the Canary Islands (i.e., hotspot volcanism), and the latter are located further north and are more removed from the African plate (Dionis et al. 2015). Eruptions are generally fissure-type events (Paris et al. 2011), with the most recent activity in 2014. The geological and geomorphological history of the island is marked by large landslides around the principal vent, the scars of which are visible in satellite images (Masson et al. 2008). Volcanic emissions have tendency to be sulfur-rich (Hernández et al. 2015).

Samples were taken from deposits located around the current summit and correspond to an eruption in 1995. Samples are dark in color and have very homogeneous dimensions (<10 mm in length, 20 mm in width, and 5–10 mm in thickness). Based on the TAS classification diagram, the samples can be classified as tephrite. Texturally, the Pico Do Fogo samples show high porosity and sphericity, with a large number of vesicles.

3.3 Volcanoes around Sicily, Italy

Sicily is located in a tectonically complex area related to the collision of the African and Eurasian plates. In the east, the volcanic context is that of back-arc islands (e.g., Vulcano and Stromboli). However, the origins of Mt. Etna remain a subject of debate (Andronico et al. 2005; Behncke et al. 2009).

Mt. Etna is a highly active volcano located on the eastern coast of Sicily; both intermediate and basic magmas are produced. The geologic history shows overlapping volcanic cones (Branca et al. 2004; Scollo et al. 2005) and evidence for large landslides (Barbano et al. 2014). The samples used for analysis were homogeneous in shape and size, with a size of <3 mm and a dark color. Based on the TAS classification diagram, the samples can be classified as basalt. Texturally, the samples show high porosity, with large-sized interconnected vesicles.

Stromboli volcano is a back-arc volcano located in the Tyrrhenian Sea to the north of Sicily; it reflects a complex process of subduction, rifting, basin formation, and basin extension (Astis et al. 2003). In recent millennia (2000–2500 years), the volcano has been characterized by regular and low-intensity, fountaining-style eruptions interspersed by short periods of more explosive eruptions (Bertagnini et al. 2011). There is evidence for several flank collapses of the northeast face of the cone. Samples were taken from deposits emplaced in 2013; they are homogeneous in size and shape, with a size of <2 mm and a very dark color. Based on the TAS classification diagram, the samples can be classified as basalt. SEM images show that the samples are vesicle-poor, indicative of a gentle eruption style. Despite different tectonic settings, Mt. Etna and Stromboli have similar geochemical

characteristics and it has been suggested that the magma storage regions are interconnected by an enormous fracture zone (Schiano et al. 2004).

Vulcano is a back-arc volcano located in the Tyrrhenian Sea to the north of Sicily (Becaluva et al. 1985). The volcano has experienced large landslides on its flanks, and these have been associated with tsunamis (Tinti and Piatanesi 1996). Samples were taken from deposits emplaced in 1985 (Arrighi et al. 2006); they have a grayish color, heterogeneous size, and they are round and smooth. Based on the TAS classification diagram, the samples can be classified as trachyandesite; based on their high K content (wt.% 5) they can be classified as shoshonitic (Peccerillo and Taylor 1976). Texturally, the Vulcano samples show high porosity, with irregular, interconnected vesicles.

3.4 Deception Island, Antarctica

Deception Island is located close to the Antarctic Peninsula. It is one of the most dangerous and active volcanoes in the region, with more than 20 eruptions in the last two centuries (Pallàs et al. 2001; Smellie 2001). The origin of the island is related to basaltic-andesite phreatomagmatic (explosive) eruptions that produce large volumes of pyroclastic material (Marti and Baraldo 1990). The morphology of the island includes a large collapse feature associated with normal faults of tectonic origin (Weaver et al. 1979). Moreover, lahars and minor landslides are frequent during the austral summer (Ibáñez et al. 2000, 2003a, b; Carmona et al. 2012).

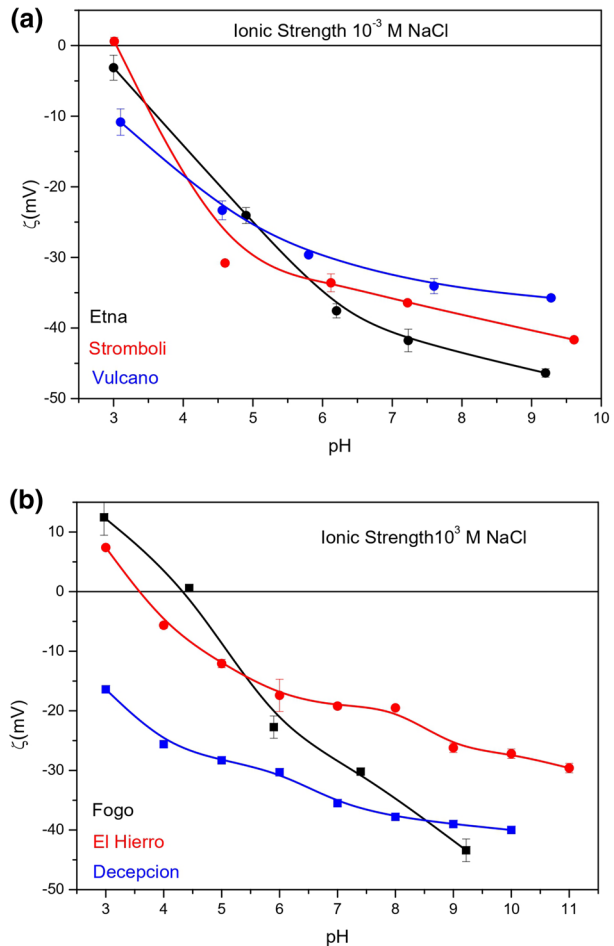
The samples chosen for analysis are very dark in color, are of gravel size, and have an rough, ellipsoidal form. The surfaces are coated in diatomaceous material (Ontiveros-Ortega et al. 2014). Based on the TAS classification diagram, the samples can be classified as basaltic-andesite. Texturally, the samples contain curved and very smooth surfaces with irregular vesicles, consistent with eruption during phreatomagmatic events characterized by rapid cooling of the magma and the sudden expulsion of gas (Lücke and Calderón 2016).

4 Results and discussion

4.1 Zeta potential

To date, only a few studies have presented systematic measurements of both the electrical and thermodynamic properties of volcanic ash particles or calculated the electrostatic interaction energies between them (Li et al. 1997; Plaza et al. 2018; Aizawa 2008; Aizawa et al. 2008; Ontiveros-Ortega et al. 2014; Kameda 2021). In Fig. 4, we show ξ values obtained for different pH values at a constant ionic strength of 1 mM of NaCl. In general, the eruptive materials have negative charge over the entire range of pH studied. Similar results have previously been obtained using electrophoretic mobility (Ontiveros-Ortega et al. 2014, 2016; Plaza et al. 2018; Holysz 2000; Wang and Revil 2010) and other electrokinetic techniques, including the streaming potential (Dultz et al. 2016; Revil et al. 2002). The negative values of zeta potential can be attributed to the nature of the functional groups on their surface, mainly those on silica (Li et al. 1997; Chibowski and Holysz 1992; Duran et al. 1998; Carre et al. 1992); as such, we chose to analyze samples from eruptions covering a range of silica contents (42–60 wt.% SiO₂). Thus, the main mechanism that could explain the negative charge of silica is the broken

Fig. 4 **a** Zeta potential (ζ) of volcanic ash. (A) Zeta potential (ζ) of volcanic ash as function of pH for a 1 mM NaCl concentration for Etna Stromboli and Vulcano (all points include error bars, although in some of them they are so small that are hidden under the points). **b** Zeta potential (ζ) of volcanic ash. (A) Zeta potential (ζ) of volcanic ash as function of pH for a 1 mM NaCl concentration for Pico do Fogo, El Hierro, and Deception Island (all points include error bars, although in some of them they are so small that are hidden under the points)



bonds of SiO_4 tetrahedra at the glass or mineral surface, giving rise to Si–OH groups, whose point of zero charge (PZC) is approximately 2 (Kim and Lawler 2005) (so, at $\text{pH} > 2$, silica would be deprotonated and negative charges would progressively increase at glass/mineral edges). The studied sample surfaces have various functional groups (e.g., Si–OH, Al–OH, Mg–OH, Fe–OH) with different points of zero charge, and the overall zeta potential measured at a given pH reflects the sum of all deprotonated and protonated groups depending on the specific sample composition. A different behavior is observed for tephrites (Pico Do Fogo and El Hierro) at acidic pH levels (Fig. 4a); the ζ was positive for the lowest pH values, probably reflecting both its lower SiO_2 content ($\approx 43\%$ wt.), which PZC is 1.0–2.0, and a greater protonation of surface Mg–OH and Fe–OH, which showed PZC ranging from 6.5 to 12.7 (Brunelle 1978). This behavior was previously described by Yang et al. (2018) for pyroxenes, one of the mineral that composes the tephrite samples. Under these pH conditions, the electrical repulsion between fine particles was the lowest identified in this study.

In general, as pH increased, all of the samples showed increases in absolute ζ , probably due to the deprotonation of OH groups on the surfaces of the particles, indicating that the

contribution of the electrical component to the cohesion of the deposit is clearly repulsive. This increase in repulsion is proportional to the increase in pH.

The absolute increase in ξ was largest for Pico Do Fogo (56 mV) and smallest for Deception Island (22.6 mV), indicating that the cohesion of an ash deposit on Pico Do Fogo can change drastically with pH, while the effect is less prominent for Deception Island deposits. Numerous studies have considered volcanic hazards on Deception Island (Bartolini et al. 2014; Geyer et al. 1019). Our results provide a novel perspective and suggest that, owing to the high cohesion of particles, landslides on Deception Island have the potential to be massive and to produce tsunamis affecting coastal areas of Antarctica, including the Deception and Gabriel de Castilla bases.

Negative charge increased (or positive charge diminished for tephrites when $\text{pH} < 3.5\text{--}4.5$) with increasing pH of the medium for all samples, but the patterns and magnitudes of change differed. We observed steeper slopes of the ξ curve for Pico Do Fogo, El Hierro, Mt. Etna, and Stromboli, and flatter slopes for Deception Island and Vulcano. Generally, the gentle slopes correspond to ash expelled during more explosive eruptions (vulcanian/phreatomagmatic) or those with a greater discharge volume (Hawaiian/strombolian). Another interesting finding is that at more basic pH, the electrostatic repulsion between particles constituting the deposit is increased, and so cohesion should be minimal.

In summary, acid pH levels, which are common in volcanic environments, decrease the repulsion between particles and favor cohesion. However, when washed by persistent rain, the pH becomes less acidic, bearing in mind the typical pH range of rainwater (< 6.0) (Suzuki et al. 2020), which favors repulsion and a decrease in cohesion. The integrity of the volcanic structure depends in part on this cohesion among particles. As such, heavy rainfall can be linked with landslides and an increased degree of erosion. From the perspective of electrostatic interaction, the deposits of El Hierro are the most stable (with the lowest repulsion among particles). At first glance, this contradicts the fact that El Hierro Island has experienced numerous landslides; however, we suggest that while the high degree of cohesion reduces the occurrence of small landslides, it facilitates massive landslides as large sectors of material slip together. At the other end, the spectrum is Mt. Etna, where deposits are more disaggregated; this is consistent with a lack of large discontinuities due to large landslides.

4.2 Surface free energy

The surface free energy of a deposit reflects the non-electrostatic interactions between particles, including van der Waals, hydrogen bonding, and structural interactions (Oss 1994).

Table 4 Values of the Lifshitz van der Waals γ^{LW} component, electron acceptor γ^+ , and electron donor γ^- parameters of the acid–base component of surface free energy, for different samples of volcanic materials

Samples/SFE	γ^{LW} (mJ/m ²)	γ^+ (mJ/m ²)	γ^- (mJ/m ²)	γ^{TOT} (mJ/m ²)
El Hierro	35 ± 2	3.8 ± 0.6	35 ± 3	35 ± 2
Fogo	72 ± 2	1.1 ± 0.3	52 ± 3	87 ± 2
Etna	52 ± 2	0.2 ± 0.3	63 ± 3	60 ± 2
Vulcano	63 ± 2	1.1 ± 0.3	38 ± 3	76 ± 2
Stromboli	50 ± 2	0.0 ± 0.3	70 ± 3	51 ± 2
Deception	46.2 ± 0.3	0.326 ± 0.003	28.8 ± 0.7	52.3 ± 0.5

In addition, it provides information on the hydrophobic and hydrophilic nature of the material, and therefore on the capacity to retain water, which increases the weight component and facilitates landslides.

From Table 4, the LW surface tension component varied significantly among the ash samples, even within the same rock type. Previous study of silicate clay minerals and other inorganic materials showed large variation in γ^{LW} components up to 10 mJ/m² (Li et al. 1997; Plaza et al. 2018; Aizawa 2008; Ontiveros-Ortega et al. 2014; Holysz 2000); in these data, silica-rich glass material showed similar variability in surface tension to that observed here (Li et al. 1997; Aizawa 2008; Ontiveros-Ortega et al. 2014).

From analysis of the dispersive component γ^{LW} , the highest values were found for Pico Do Fogo (71.6 ± 2 mJ/m²) and the lowest for El Hierro (35.2 ± 2 mJ/m²). Based on Eq. 5, dispersive interaction is increasingly attractive in nature with increasing γ^{LW} . As such, among our samples, those from El Hierro have the most ordered structure of water molecules at the solid–liquid interface (Oss et al. 1989). However, from analysis of the AB components, γ^+ and γ^- , in general, the eruptive materials were monopolar ($\gamma^+ \approx 0$) electron donors ($\gamma^- > 0$). The volcanic ash in an aqueous media behaved like a Lewis base.

Given that a material is considered hydrophobic when its electron-acceptor (γ^+) component is null and its electron-donor component (γ^-) has a value of < 28.2 mJ/m² (Oss et al. 1989), the samples from Stromboli, Mt. Etna, and Pico Do Fogo were found to be hydrophilic (strong water retention) owing to electron-donor values of > 50 mJ/m². Other studies have found volcanic ash surfaces to be hygroscopic and covered by a monolayer of adsorbed water under ambient conditions (Delmelle et al. 2005; Lathem et al. 2011). However, materials from El Hierro and Vulcano had a less hydrophilic character ($\gamma^- < 40$ mJ/m²), while Deception Island samples, with $\gamma^- = 28.8 \pm 0.7$ mJ/m², showed an essentially hydrophobic character.

Deception Island is the location of both glaciers and permafrost, which provide a large volume of water to deposits, especially in summer. In recent years, this phenomenon has been aggravated by climate change. However, if we consider that our results for the samples studied are representative of the deposits, we can say that the deposits on Deception Island are unable to retain a large amount of water; as such, landslides driven by increased water weight are not a significant risk to the scientific bases and tourists infrastructure on the island. In contrast, deposits on Stromboli have high hydrophilicity, indicating a large capacity for water retention and increased risk of water-driven landslides.

4.3 Total interaction energy

The interaction between particles within a deposit is the sum of the electrical, dispersive, and non-dispersive contributions. As such, the cohesion and stability of volcanic deposits reflect a combination of the factors discussed above; no single line of evidence can be taken in isolation when predicting macroscopic stability or the rheological behavior of terrestrial deposits.

Figure 5a shows the total interaction energy as a function of distance H , calculated as the sum of three components shown in Fig. 5b–d. The electrical component (EL) between equal particles is always positive and constitutes a potential barrier (repulsive interaction). The acid–base interaction (AB) between equal particles will always be repulsive, although between different particles it can be attractive, negative, or even oscillate between these two extremes. Although both the electrical and polar

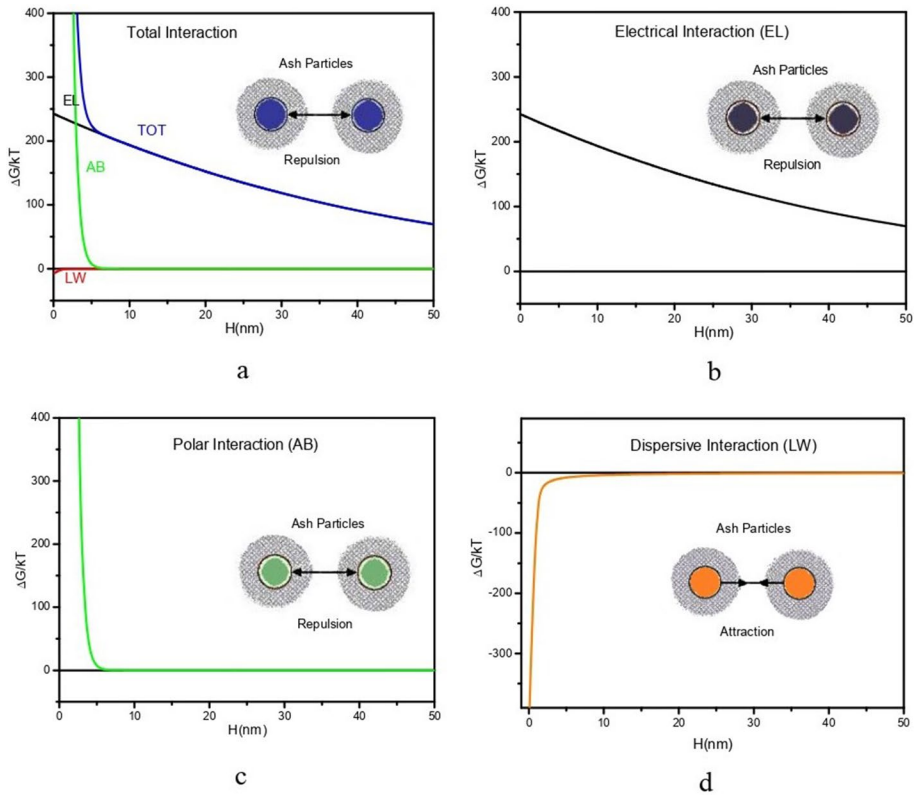


Fig. 5 Graphical representation of the interaction energy between ash particles (in kT). **A** Total energy of interaction, **B** electrical component, **C** polar component, and **D** dispersive component

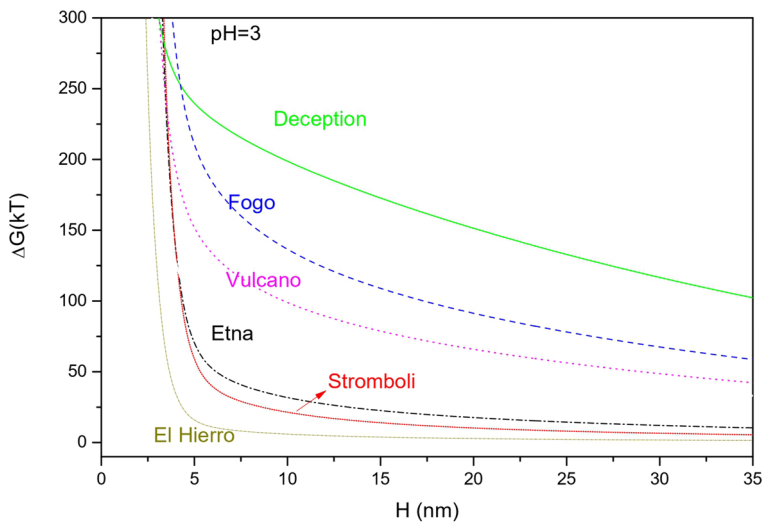


Fig. 6 Total energy of interaction (in kT) between particles as a function of the distance between surfaces, H , for a pH of 3 and a 1 mM NaCl concentration

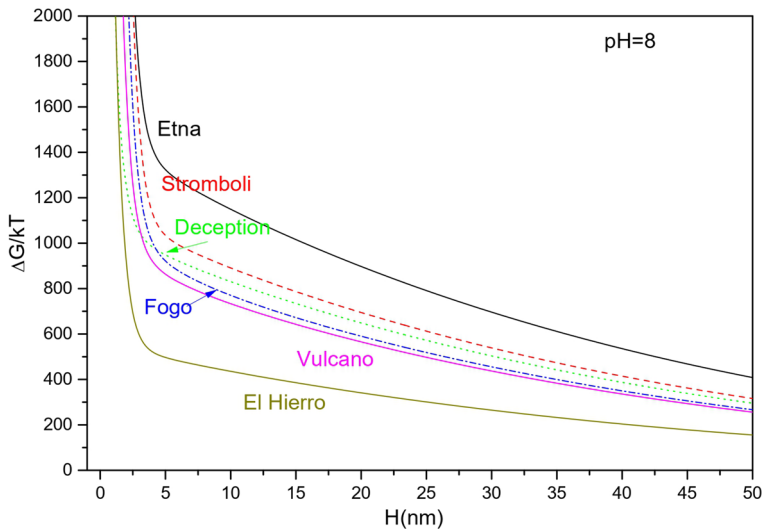


Fig. 7 Total energy of interaction (in kT) between particles as a function of the distance between surfaces, H , for a pH of 8 and a 1 mM NaCl concentration

components are repulsive, the AB component acts over shorter distances, such that it is especially decisive under conditions where electrical interaction is negligible, pH is highly acidic, and/or the ionic force is high.

Figures 6 and 7 show the total interaction energies between ash particles as a function of the separation distance (H) between the particles and the ξ (Fig. 4) and surface free energy components (Table 4) based on Eqs. 2, 3, and 6. This interaction energy is presented for two pH situations: (1) a very acidic environment (i.e., the usual scenario during and after an eruptive episode), pH = 3 (Fig. 6); and (2) a basic environment, pH = 8 (Fig. 7).

From Fig. 6, we identified two different behaviors: a group for which the potential barriers are < 50 kT for $H > 10$ nm, and another for which they are around 250 kT for $H > 10$ nm. In this acidic environment (pH = 3), important barriers of potential appear (~ 900 kT), and so there is net repulsion between the particles that make up the substrate (i.e., weak cohesion and therefore instability). If the studied samples are representative of the deposits more widely, the potential energy values show that El Hierro, Stromboli, and Mt. Etna are the most cohesive volcanic structures and therefore, to a first approximation, the most stable. In contrast, Pico Do Fogo and Deception Island present the greatest instability.

Figure 7 shows the values obtained for volcanic materials studied at pH = 8. The values obtained for the interaction energy barriers (700–1000 kT) are higher than those at pH = 3. The values obtained for potential energy avoid an approximation between the particles smaller than 50 nm and thus prevent effective cohesion.

Our results show that ash cohesion at Mt. Etna and Stromboli is strongly pH dependent, while that at El Hierro is much less dependent. We believe that this reflects the greater age of deposits at El Hierro (10,000 years), which has provided sufficient time for mineral breakdown owing to weathering, altering the surface properties of the material.

5 Conclusions and outlook

We present one of the first comparative studies of microscopic surficial interactions between particles in volcanic deposits and consider the potential implications for macroscopic processes (e.g., landslides). Our results, based on a small number of samples from six different volcanoes, demonstrate that studying both the electrical and thermodynamic properties of eruptive materials facilitates the determination of deposit cohesion.

Electrical properties analysis shows that eruptive materials from a range of different volcanic environments all have a negative charge in aqueous solution, reflecting the large silica component in volcanic products. Negative zeta potential increases with increasing pH, indicating that cohesion decreases drastically when pH increases. On this basis, studied samples from El Hierro and Vulcano are the most cohesive among the samples studied, while those from Pico Do Fogo and Mt. Etna are the least cohesive. In terms of surface free energy, some deposits are hydrophobic (e.g., those from Deception Island), while others are hydrophilic (e.g., those from Pico Do Fogo). Hydrophilicity was the most common characteristic among our samples.

Our calculation of interaction energy confirms that deposit cohesion varies among volcanoes, and that this cohesion changes drastically with the pH of the medium. At acidic pH (pH = 3), El Hierro materials are the most cohesive followed by Stromboli, Mt. Etna, Vulcano, Pico Do Fogo, and Deception Island. At basic pH (pH = 8), El Hierro materials continue to be the most cohesive followed by Vulcan, Pico Do Fogo, Deception Island, Stromboli, and Mt. Etna.

This preliminary study focused on a small number of samples from just six volcanoes. Volcanoes produce a variety of materials, even within the same eruptive episode; moreover, samples from different environments and of different ages undergo hugely variable post-eruptive alteration (e.g., weathering, hydrothermal). As such, our results cannot be considered comprehensive or predictive for any given volcano. However, they do suggest the importance of microscopic electrical and thermodynamic properties on the stability of volcanic deposits and confirm the need to include cohesion studies when considering the stability of volcanic deposits. The analysis of interfacial interactions between particles has significant implications for factors such as water retention, and as such is important for the prediction of landslide hazards around volcanic structures. We believe that our study provides an important proof of concept, and that this area of research requires significant further study.

Acknowledgements This is a short text to acknowledge the contributions of specific colleagues, institutions, or agencies that aided the efforts of the authors. Technical and human support provided by Centro de Instrumentación Científico-Técnica (CICT)—Servicios Centrales de Apoyo a la Investigación (SCAI)—Universidad de Jaén (UJA, MICINN, Junta de Andalucía, FEDER) is gratefully acknowledged.

Author contributions The author contributions section is mandatory for all articles, including articles by sole authors. If an appropriate statement is not provided on submission, a standard one will be inserted during the production process. The author contributions statement must describe the contributions of individual authors referred to by their initials, and in doing so, all authors agree to be accountable for the content of the work. Please see here for full authorship criteria.

Funding Funding for open access publishing: Universidad de Jaén/CBUA. This work was partially funded by the Spanish MINECO Project FEMALE, PID2019-106260GB-I00. Funding for open access charge: Universidad de Jaén.

Data availability statement The datasets [GENERATED/ANALYZED] for this study can be found in the [NAME OF REPOSITORY] [LINK]. Please see the Data Availability section of the Author guidelines for more details.

Declaration

Conflict of interest The authors declare that the research was conducted in the absence of any commercial or financial relationships that could be construed as a potential conflict of interest.

Open Access This article is licensed under a Creative Commons Attribution 4.0 International License, which permits use, sharing, adaptation, distribution and reproduction in any medium or format, as long as you give appropriate credit to the original author(s) and the source, provide a link to the Creative Commons licence, and indicate if changes were made. The images or other third party material in this article are included in the article's Creative Commons licence, unless indicated otherwise in a credit line to the material. If material is not included in the article's Creative Commons licence and your intended use is not permitted by statutory regulation or exceeds the permitted use, you will need to obtain permission directly from the copyright holder. To view a copy of this licence, visit <http://creativecommons.org/licenses/by/4.0/>.

References

- Aizawa K (2008) Classification of self-potential anomalies on volcanoes and possible interpretations for their subsurface structure. *J Volcanol Geotherm Res* 175:253–268
- Aizawa K, Uyeshima M, Nogami K (2008) Zeta potential estimation of volcanic rocks on 11 island arc-type volcanoes in Japan: implication for the generation of local self-potential anomalies. *J Geophys Res* 113:B02201. <https://doi.org/10.1029/2007JB005058>
- Ancochea E, Fuster J, Ibarrola E, Cendrero A, Coello J, Hernan F et al (1990) Volcanic evolution of the island of Tenerife (Canary Islands) in the light of new K-Ar data. *J Volcanol Geotherm Res* 44(3):231–249
- Andronico D, Branca S, Calvari S, Burton M, Caltabiano T, Corsaro RA et al (2005) A multi-disciplinary study of the 2002–03 Etna eruption: insights into a complex plumbing system. *Bull Volc* 67:314–330
- Arrighi S, Tanguy J-C, Rosi M (2006) Eruptions of the last 2200 years at Vulcano and Vulcanello (Aeolian Islands, Italy) dated by high-accuracy archeomagnetism. *Phys Earth Planet Int* 159:225–233
- Bailey SW, Brousseau PA, McGuire KJ, Ross DS (2014) Influence of landscape position and transient water table on soil development and carbon distribution in a steep, headwater catchment. *Geoderma* 226:279–289
- Balcells R, Gomez JA. *Memorias y mapas geológicos del Plan MAGNA. 1:25000. El Hierro, Hoja de Frontera: Instituto Geológico y Minero de España, España; 1997b (in Spanish).*
- Barbano MS, Pappalardo G, Pirrotta C, Mineo S (2014) Landslide triggers along volcanic rock slopes in eastern Sicily (Italy). *Nat Hazards* 73(3):1587–1607
- Bartolini S, Geyer A, Martí J, Pedrazzi D, Aguirre-Díaz G (2014) Journal volcanic hazard on Deception Island (South Shetland Islands, Antarctica). *J Volcanol Geotherm Res* 285:150–168
- Baumgarten W, Dörner J, Horn R (2013) Microstructural development in volcanic ash soils from South Chile. *Soil Tillage Res* 129:48–60
- Beccaluva L, Gabbianelli G, Lucchini F, Rossi PL, Savelli C (1985) Petrology and K/Ar ages of volcanics dredged from the Eolian seamounts: implications for geodynamic evolution of the southern Tyrrhenian basin. *Earth Planet Sci Lett* 74(2):187–208
- Behncke B, Falsaperla S, Pecora E (2009) Complex magma dynamics at Mount Etna revealed by seismic, thermal, and volcanological data. *J Geophys Res Solid Earth* 114(B3):B03211
- Bertagnini A, Di Roberto A, Pompilio M (2011) Paroxysmal activity at Stromboli: lessons from the past. *Bull Volcanol* 73(9):1229–1243
- Bommer JJ, Rolo R, Mitroulia A, Berdousis P (2002) Geotechnical properties and seismic slope stability of volcanic soils. In: *Proceedings of the 12th European conference on earthquake engineering (London, UK)*, Paper No. 695
- Branca S, Coltelli M, Groppelli G (2004) Geological evolution of Etna volcano. In Bonaccorso, A., Calvari, S., Coltelli, M., Del Negro, C., Falsaperla, S. (Eds.), *Mt. Etna: Volcano Laboratory* (pp. 49–63). Washington, DC: American Geophysical Unions Geophysical Monograph Series.

- Brunelle JP (1978) Preparation of catalysts by metallic complex adsorption on mineral oxides. *Pure Appl Chem* 50:1211–1229
- Carmona E, Almendros J, Serrano I, Stich D, Ibáñez JM (2012) Results of seismic monitoring surveys of Deception Island volcano, Antarctica, from 1999–2011. *Antarct Sci* 24:1–15. <https://doi.org/10.1017/S0954102012000314>
- Carracedo JC, Pérez Torrado FJ, Ancochea E, Meco J, Hernán F, Cubas CR et al (2002) Cenozoic volcanism II: the Canary Islands. Geological Society of London, London
- Carre A, Roger F, Varinot C (1992) Study of acid/base properties of oxide, oxide glass, and glass-ceramic surfaces. *J Colloid Interface Sci* 154(1):174–183
- Chibowski E (1992) Solid surface free energy components determination by the thin-layer wicking technique. *J Adhes Sci Technol* 6(9):1069e90
- Chibowski E, Holysz L (1992) Use of the Washburn equation for surface free energy determination. *Langmuir* 8(2):710–716
- De Astis G, Ventura G, Vilardo G (2003) Geodynamic significance of the Aeolian volcanism (Southern Tyrrhenian Sea, Italy) in light of structural seismological, and geochemical data. *Tectonics* 22(4):1040
- Delmelle P, Villieras F, Pelletier M (2005) Surface area, porosity and water adsorption properties of fine volcanic ash particles. *Bull Volcanol* 67:160–169
- Dionis SM, Melián G, Rodríguez F, Hernández PA, Padrón E, Pérez NM (2015) Diffuse volcanic gas emission and thermal energy release from the summit crater of Pico do Fogo, Cape Verde, 27 January 2015. *Bull Volcanol* 77:10
- Dultz S, Behrens H, Hensch G, Deubener J (2016) Electrolyte effects on surface chemistry of basaltic glass in the initial stages of dissolution. *Chem Geol* 426:71–84
- Duran JDG, Ontiveros A, Delgado AV, Gonzalez-Caballero F (1998) Kinetics and interfacial interactions in the adhesion of colloidal calcium carbonate to glass in a packed-bed. *Appl Surf Sci* 134(1):125–138
- Geyer A, Álvarez-Valero AM, Gisbert G, Aulinas M, Hernández-Barreña D, Lobo A et al (2019) Deciphering the evolution of Deception Island's magmatic system. *Nat Sci Rep* 9:373. <https://doi.org/10.1038/s41598-018-36188-4>
- Gimmi T, Kosakowski G (2011) How mobile are sorbed cations in clays and clay rocks? *Environ Sci Technol* 45(4):1443–1449
- Guillou H, Carracedo JC, Torrado FP, Badiola ER (1996) K-Ar ages and magnetic stratigraphy of a hotspot-induced, fast grown oceanic island: El Hierro, Canary Islands. *J Volcanol Geotherm Res* 73(1–2):141–155
- Hernández PA, Melián G, Dionis SM, Barrancos J, Padilla G, Padrón E et al (2015) Chemical composition of volcanic gases emitted during the 2014–15 Fogo eruption, Cape Verde. EGU General Assembly 2015
- Holtz RD, Kovacs WD, Sheahan TC (1981) An introduction to geotechnical engineering. Pearson, London
- Holysz L (2000) Investigation of the effect of substrata on the surface free energy components of silica gel determined by thin layer wicking method. *J Mater Sci* 35:6081–6091. <https://doi.org/10.1016/j.biomaterials.2005.11.014>
- Ibáñez JM, Del Pezzo E, Almendros J, La Rocca M, Alguacil G, Ortiz R et al (2000) Seismovolcanic signals at deception island volcano, Antarctica: wave field analysis and source modeling. *J Geophys Res* 105:13905–13931
- Ibáñez JM, Almendros J, Carmona E, Martínez-Arévalo C, Abril M (2003a) The recent seismo-volcanic activity at Deception Island volcano. *Deep-Sea Res II* 50:1611–1629
- Ibáñez JM, Carmona E, Almendros J, Saccorotti G, Del Pezzo E, Abril M et al (2003b) The 1998–1999 seismic series at Deception Island volcano, Antarctica. *J Volcanol Geotherm Res* 128:65–88
- Kadar E, Fisher A, Stolpe B, Calabrese S, Lead J, Valsami-Jones E et al (2014) Colloidal stability of nanoparticles derived from simulated cloud-processed mineral dusts. *Sci Total Environ* 466:864–870
- Kameda J (2021) Mineralogical and physico-chemical properties of halloysite-bearing slip surface material from a landslide during the 2018 Eastern Iburi earthquake, Hokkaido. *Prog Earth Planet Sci* 8:37
- Kelly LC, Cockell CS, Piceno YM, Andersen GL, Thorsteinsson T, Marteinsson V (2010) Bacterial diversity of weathered terrestrial Icelandic volcanic glasses. *Microb Ecol* 60(4):740–752
- Kim J, Lawler D (2005) Characteristics of zeta potential distribution in silica particles. *Bull Korean Chem Soc* 26:1083–1090
- Latham TL, Kumar P, Nenes A, Dufek J, Sokolik IN, Trail M, Russell A (2011) Hygroscopic properties of volcanic ash. *Geophys Res Lett* 38:L11802
- Li Z, Giese RF, Wul W, Sheridan MF, van Oss CJ (1997) The surface thermodynamic properties of some volcanic ash colloids. *J Disp Sci Technol* 18(3):223–241

- Lücke O, Calderón A (2016) Characterization of the ashes from the 2014–2015 Turrialba Volcano eruption by means of Scanning Electron Microscopy and Energy Dispersive X-Ray Spectroscopy. *Revista Geológica De América Central* 54:109–123
- Marti J, Baraldo A (1990) Pre-caldera pyroclastic deposits of Deception Island (South Shetland Islands). *Antarct Sci* 2:345–352
- Masson DG, Le Bas TP, Grevemeyer I, Weinrebe W (2008) Flank collapse and large-scale landsliding in the Cape Verde Islands, off West Africa. *Geochem Geophys Geosyst* 9(7):Q07015
- Maters EC, Delmelle P, Rossi MJ, Ayris PM, Bernard A (2016) Controls on the surface chemical reactivity of volcanic ash investigated with probe gases. *Earth Planet Sci Lett* 450:254–262
- Ontiveros-Ortega A, Vidal F, Gimenez E, Ibáñez JM (2014) Effect of heavy metals on the surface free energy and zeta potential of volcanic glass: implications on the adhesion and growth of microorganisms. *J Mater Sci* 49(9):3550–3559
- Ontiveros-Ortega A, Moleon JA, Plaza I, Guillén C (2016) Effect of interfacial properties on mechanical stability of ash deposit. *J Rock Mech Geotech Eng* 8(2):187–197
- Ontiveros-Ortega E, Ruiz-Agudo EM, Ontiveros-Ortega A (2018) Thermal decomposition of the CaO in traditional lime kilns. Application in cultural heritage conservation. *Constr Build Mater* 190:349–362
- Pallàs R, Smellie JL, Casas JM, Calvet J (2001) Using tephrochronology to date temperate ice: correlation between ice tephros on Livingston Island and eruptive units on Deception Island volcano (South Shetland Islands, Antarctica). *Holocene* 11(2):149–160
- Paris R, Giachetti T, Chevalier J, Guillou H, Frank N (2011) Tsunami deposits in Santiago Island (Cape Verde archipelago) as possible evidence of a massive flank failure of Fogos volcano. *Sediment Geol* 239:129–145
- Peccerillo A, Taylor SR (1976) Geochemistry of Eocene calc-alkaline volcanic rocks of the Kastamonu area, northern Turkey. *Contrib Mineral Petrol* 58:63–81
- Plaza I, Ontiveros-Ortega A, Calero J, Aranda V (2015) Implication of zeta potential and surface free energy in the description of agricultural soil quality: effect of different cations and humic acids on degraded soils. *Soil Tillage Res* 146:148–158
- Plaza I, Ontiveros-Ortega A, Calero J, Romero C (2018) A new approach to triggering mechanism of volcano landslides based on zeta potential and surface free energy balance. *Geomorphology* 301:1–9
- Revil A, Hermitte D, Spangenberg E, Cochemé JJ (2002) Electrical properties of zeolitized volcanoclastic materials. *J Geophys Res* 107(B8):2168. <https://doi.org/10.1029/2001JB000599>
- Schiano P, Clocchiatti R, Ottolini L, Sbrana A (2004) The relationship between potassic, calc-alkaline and Na-alkaline magmatism in South Italy volcanoes: a melt inclusion approach. *Earth Planet Sci Lett* 220:121–137
- Scollo S, Cottelli M, Prodi F, Folegani M, Natali S (2005) Solid Earth-L10302-Terminal settling velocity measurements of volcanic ash during the 2002–2003 Etna eruption by an X-band microwave rain gauge disdrometer. *Geophys Res Lett*. <https://doi.org/10.1029/2004GLO22100>
- Siebert L, Simkin T, Kimberly P (2010) Volcanoes of the world, 3rd edn. Smithsonian Institution, Washington, DC; University of California Press, Berkeley, p 551
- Smellie JL (2001) Lithostratigraphy and volcanic evolution of deception island, South Shetland Islands. *Antarct Sci* 13(02):188–209
- Smoluchowski MV (1921) Elektroosmosis. *Handbuch der Elektrizität und des Magnetismus* (Leipzig, Barth Verlag), p 366
- Suzuki T, Nakase K, Tamenishi T, Niinae M (2020) Influence of pH and cations in Rainwater on leaching of Cd(II) from artificially contaminated montmorillonite. *J Environ Chem Eng* 8(5):10408
- Tinti S, Piatanesi A (1996) Numerical simulations of the tsunami induced by the 1627 earthquake affecting Gargano, Southern Italy. *J Geodyn* 21(2):141–160
- van Oss CJ (1994) Polar or Lewis acid–base interactions. In: *Interfacial forces in aqueous media*. CRC Press, pp 18–46
- van Oss CJ, Chaudhury MA, Good RJ (1988) Interfacial Lifshitz-van der Waals and polar interactions in macroscopic systems. *Chem Rev* 88(6):927–941
- van Oss CJ, Ju L, Chaudhury MK, Good RJ (1989) Estimation of the polar parameters of the surface tension of liquids by contact angle measurements on gels. *J Colloid Interface Sci* 128(2):313–319
- Voight B, Elsworth D (1997) Failure of volcano slopes. *Geotechnique* 47(1):1–31
- Wang M, Revil A (2010) Electrochemical charge of silica surfaces at high ionic strength in narrow channels. *J Colloid Interface Sci* 343:381–383
- Washburn EW (1921) The dynamics of capillary flow. *Phys Rev* 17(3):273
- Weaver SD, Saunders AD, Pankhurst RJ, Tarney J (1979) A geochemical study of magmatism associated with the initial stages of back-arc spreading. *Contr Mineral Petrol* 68:151–169

Yang S, Xie B, Lu Y, Li C (2018) Role of magnesium-bearing silicates in the flotation of pyrite in the presence of serpentines limes. *Powder Technol* 332:1–7

Publisher's Note Springer Nature remains neutral with regard to jurisdictional claims in published maps and institutional affiliations.